

©2011 American Physical Society. Access to this work was provided by the University of Maryland, Baltimore County (UMBC) ScholarWorks@UMBC digital repository on the Maryland Shared Open Access (MD-SOAR) platform.

Please provide feedback

Please support the ScholarWorks@UMBC repository by emailing scholarworks-group@umbc.edu and telling us

what having access to this work means to you and why it's important to you. Thank you.

Role of pump coherence in two-photon interferometry

J. Liang, S. M. Hendrickson, and T. B. Pittman

Physics Department, University of Maryland Baltimore County, Baltimore, Maryland 21250, USA

(Received 20 December 2010; published 10 March 2011)

We use a parametric down-conversion source pumped by a short-coherence-length continuous-wave (CW) diode laser to perform two-photon interferometry in an intermediate regime between the more familiar Franson-type experiments with a long-coherence-length pump laser, and the short pulsed pump “time-bin” experiments pioneered by Gisin’s group. The use of a time-bin-like Mach-Zehnder interferometer in the CW pumping beam induces coherence between certain two-photon amplitudes, while the CW nature of the experiment prevents the elimination of remaining incoherent ones. The experimental results highlight the role of pump coherence in two-photon interferometry.

DOI: [10.1103/PhysRevA.83.033812](https://doi.org/10.1103/PhysRevA.83.033812)

PACS number(s): 42.65.Lm, 42.50.St, 42.50.Dv

I. INTRODUCTION

Two-photon interferometry is a rapidly growing field with applications ranging from metrology [1,2] and secure communications [3] to fundamental tests of quantum mechanics [4]. When the two-photon state is produced by parametric down-conversion (PDC) [5], it is well-known that the coherence properties of the laser pumping the PDC source play an important role. The original Franson interferometer experiments [6] represent one extreme, where a long-coherence-length continuous-wave (CW) pump laser is used to produce a PDC photon pair whose emission time is essentially undefined. In the other extreme, Gisin’s time-bin entanglement experiments [7] utilize a single short pump pulse passing through an unbalanced Mach-Zehnder (MZ) interferometer to produce a PDC photon pair whose emission time is a coherent superposition of two well-defined values.

In this paper we provide an explicit experimental demonstration of an intermediate regime, where a short-coherence-length CW pump laser is passed through a Gisin-type MZ pump interferometer. This produces a PDC photon pair in a coherent superposition of two time values with a well-defined separation, but an unknown overall starting time. The coherence generated between two distinct creation times allows a recovery of certain two-photon interference effects that would otherwise be nonexistent with a short-coherence-length CW pump, while the incoherent nature of the possible starting times limits the maximum visibility of these interference effects to 50%.

This work builds on several earlier PDC experiments in which two-photon interference effects originate from the possibility of multiple arrival times of a given pump photon at the PDC source. For example, Burlakov *et al.* used a CW helium-cadmium laser possessing several randomly phased longitudinal modes which interfere to produce a series of repetitive spikes in the pump photon amplitude [8]. Similar effects were observed by Kwon *et al.* using a low-cost multimode diode laser as a pump [9]. Other related work involves the coherence between two subsequent pump pulses from a mode-locked laser [10–12], and higher-order time-bin entanglement generated by a coherent pulse train [13,14].

II. OVERVIEW

A conceptual overview of the experiment is shown in Fig. 1. A PDC source emits photons into opposite ports of a 50:50 beamsplitter in a typical Hong-Ou-Mandel (HOM) interferometer arrangement [15,16]. The HOM interference effect causes both photons to leave in the same output port, which produces a two-photon maximally path-entangled NOON ($|N,0\rangle + |0,N\rangle$) state [17] in the output modes. The outputs of the HOM beamsplitter are then recombined at a second 50:50 beamsplitter, thereby forming a PDC MZ interferometer of the kind first developed by Rarity *et al.* [18]. In order to demonstrate the effects of interest here, we modify Rarity’s balanced MZ interferometer by including a very large path-length imbalance, denoted by τ in Fig. 1. The value of τ is chosen to be much greater than the coherence times of PDC photons as well as the pump laser. The setup is completed by the inclusion of a Gisin-type MZ pump interferometer, whose path-length imbalance τ_p is carefully matched to τ . The experiment is conducted by recording the coincidence counting rate between detectors D_1 and D_2 as a function of the relative phase difference of the interferometers.

Typical Franson-type or time-bin entanglement experiments require two spatially separated PDC MZ interferometers to study nonlocal correlations of distant photons [6,19,20]. However, many key features of the role of pump coherence in two-photon interferometry can be explored in a less stringent setting using only one common PDC MZ interferometer. In many cases, the use of a single interferometer can simplify the experiments, while still allowing the essential physics to be demonstrated. This idea has been used in some of the earliest experimental work on two-photon interferometry [21,22].

For our purposes, the use of a two-photon NOON state in the single unbalanced PDC MZ interferometer of Fig. 1 simplifies the experimental requirements in two ways. First, it reduces the number of unbalanced MZ interferometers which must be experimentally stabilized and phase-controlled. Second, the photon-bunched form of the NOON state eliminates the need to electronically “cut off” joint detection events corresponding to distinguishable two-photon amplitudes associated with one PDC photon traveling a long path while its twin takes a short path through an unbalanced MZ interferometer. For a given PDC source, this effectively doubles the coincidence counting

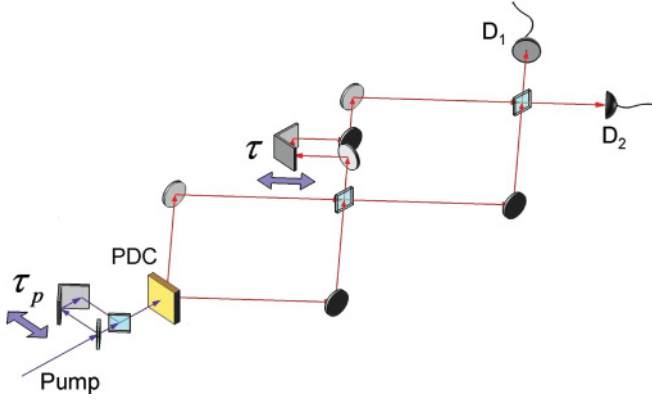


FIG. 1. (Color online) Overview of the parametric down-conversion (PDC) experiment used for two-photon interferometry in an intermediate regime between the original Franson-type experiments with a narrow-band continuous-wave (CW) pump laser [6], and the Gisin time-bin-type experiments with a short pulse as a pump [7]. Here, the PDC source is pumped by a short-coherence-length CW laser, and two sequential unbalanced Mach-Zehnder interferometers are used to experimentally demonstrate the role of pump coherence.

rate compared to the case of two separately seated PDC MZ interferometers. As can be seen from Fig. 1, when $\tau_p = \tau$ this leaves an output state with exactly four indistinguishable terms contributing to a coincidence count between D_1 and D_2 at some time t :

$$|\Psi\rangle = \frac{1}{2} \{ e^{i[\phi_o(t'-\tau)+\phi]} |S_p; L_s L_i\rangle + e^{i[\phi_o(t'-\tau)+\phi_p]} |L_p; S_s S_i\rangle + e^{i[\phi_o(t')]} |S_p; S_s S_i\rangle + e^{i[\phi_o(t'-2\tau)+\phi_p+\phi]} |L_p; L_s L_i\rangle \}. \quad (1)$$

In this simplified notation, the first ket $|S_p; L_s L_i\rangle$ denotes the pump photon traveling through the short arm of the pump interferometer, while the signal and idler photons of the PDC pair take the long path through the PDC MZ interferometer. In analogy, the final three kets in Eq. (1) correspond to the three other possible combinations of long and short paths through the two interferometers.

Each of the four indistinguishable amplitudes in Eq. (1) has a different relative phase. For simplicity, we use ϕ_p to represent the relative phase difference of the long vs. short arm in the pump interferometer. Analogously, ϕ corresponds to the “long-short” relative phase difference in the PDC MZ interferometer. In our setup, the phase ϕ represents the accumulated relative phase difference of a two-photon NOON state in the PDC MZ interferometer, with a period corresponding to the biphoton de Broglie wavelength [18,23–25].

The term ϕ_o describes the initial phase of the pump laser. Because we are using a short-coherence-length CW pump, the time dependence of ϕ_o plays a particularly important role. For a coincidence detection event at time t , we use $\phi_o(t')$ to denote the value of the pump laser phase at an earlier time $t' = t - x/c$, where x is the overall optical path length through the device via the short arms of both MZ interferometers. The first and second terms in Eq. (1) correspond to an overall extra delay of τ (e.g., propagation through the long arm of only one MZ interferometer) and therefore contain the initial pump phase $\phi_o(t' - \tau)$. Likewise, the fourth term corresponds to

propagation through the long arm of both MZ interferometers and thus contains the initial pump phase at an even earlier time, $\phi_o(t' - 2\tau)$.

Because $c\tau$ is intentionally set to be much greater than the coherence length of the pump laser, the value of $\phi_o(t' - \tau)$ will have no definite relation to $\phi_o(t')$ [or $\phi_o(t' - 2\tau)$]. Consequently, the first and second terms in Eq. (1) can interfere [7], but the third and fourth terms provide an incoherent background which limits the visibility of the two-photon interference effects.

It is instructive to use Eq. (1) to compare this intermediate regime of two-photon interferometry using a short-coherence-length CW pump, with the extreme cases of Gisin’s time-bin method using a short pumping pulse and traditional Franson interferometry with long-coherence-length CW pumps. In the time-bin case, the use of a single well-defined short pump pulse provides a “starting clock” for the experiments [7]. This provides timing information which allows the third and fourth terms in Eq. (1) to be easily discarded based on the detector firing times. The remaining first and second terms in Eq. (1) are indistinguishable in time, and share a common pump phase regardless of the coherence properties of the pump pulse. In this way, the use of a pump MZ interferometer cleverly induces the required second-order coherence, and 100% visibility two-photon interference effects can be observed with a short pulsed pump [7,13,20].

On the other extreme, Franson-type interferometry without a pump MZ results in only two terms, rather than the four listed in Eq. (1). These two terms correspond to both photons taking the long paths (e.g., $|L_s L_i\rangle$) or both taking the short paths (e.g., $|S_s S_i\rangle$) through the PDC MZ interferometer. In this case the long-long term has the relevant pump phase $\phi_o(t' - \tau)$, while the short-short term corresponds to the initial pump phase $\phi_o(t')$. However, by using a CW pump with a coherence length much greater than $c\tau$, these two terms remain coherent, and 100% visibility two-photon interference effects can be observed [6]. In this case, the required second-order coherence originates from the pump laser itself.

In the intermediate regime demonstrated here, the lack of second-order coherence due to the short coherence length of the pump is overcome to some extent by the addition of the pump MZ interferometer. For any point in time, the use of the long and short arms in the pump MZ provides two distinct points in the CW pump beam that share a common value of initial pump phase $\phi_o(t)$. Matching the separation τ_p of these two points to the delay τ in the PDC MZ results in the first two indistinguishable two-photon amplitudes in Eq. (1), in exact analogy to the pulsed time-bin case. However, the CW nature of the pump precludes the use of a “starting clock” to cut off the remaining two terms which provide an incoherent background.

Under otherwise ideal experimental conditions, this incoherent background limits the two-photon interference visibility to 50%. It can be shown that the four-term state in Eq. (1) leads to a coincidence counting rate given by

$$R_c = 1 - \frac{1}{2} \cos(\phi_p - \phi), \quad (2)$$

where the factor of 1/2 is the visibility. Because the phase shift ϕ corresponds to the NOON state de Broglie wavelength [25],

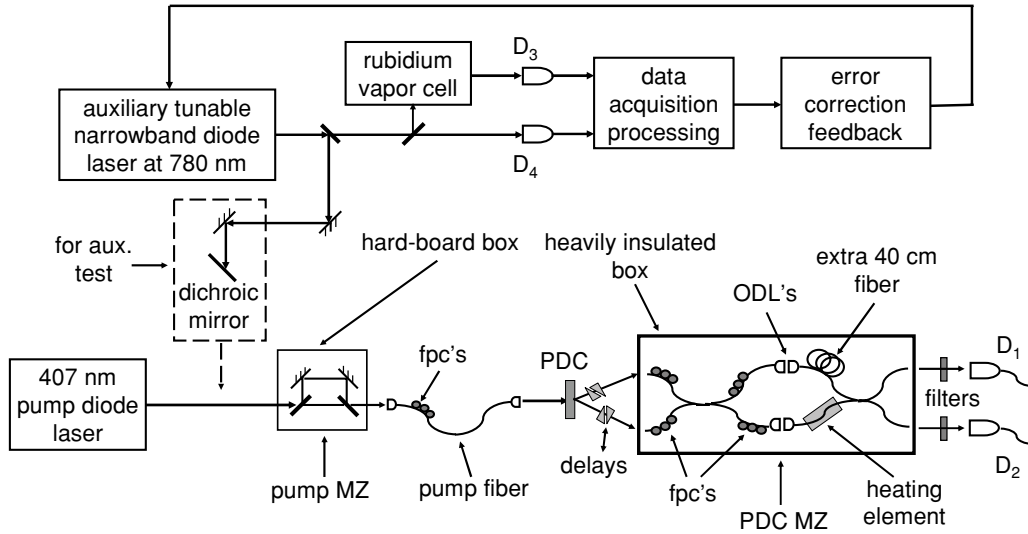


FIG. 2. Experimental apparatus used to implement the conceptual diagram of Fig. 1. Here the pump Mach-Zehnder interferometer is realized using bulk free-space optics, while the PDC Mach-Zehnder interferometer is comprised of single-mode fiber components. The upper part of the figure shows an auxiliary frequency-stabilized narrow-band laser system that is used to calibrate and test the stability and phase-scanning of the pump and PDC interferometers. The PDC source (a BBO crystal) is pumped by a short-coherence-length ultraviolet diode laser at 407 nm. The experimental studies consist of monitoring the PDC coincidence counting rate between two single photon detectors D_1 and D_2 . Additional details and symbols are found in the main text.

the coincidence counting rate is expected to show oscillations at the pump wavelength as a function of the relative path lengths in the PDC MZ interferometer.

III. EXPERIMENTAL SETUP

Figure 2 shows a schematic diagram of the apparatus we used to implement the scheme of Fig. 1. A CW ultraviolet diode laser beam (~ 40 mW at 407 nm, 0.1-nm linewidth) was sent through a free-space pump MZ comprised of two 50:50 beamsplitters and two mirrors. The pump MZ had a path-length imbalance of approximately $c\tau_p = 60$ cm. The beam coming out of one output port of the pump MZ was coupled into a single-mode pump fiber. The use of a single-mode pump fiber facilitated alignment of the free-space pump MZ interferometer and provided a convenient and robust way to deliver the pump beam to the PDC crystal. Due to losses in the pump MZ, and a nonideal transverse mode shape of the diode laser pump, the output of this fiber was typically ~ 15 mW. This free-space output was then focused into a 0.7-mm-thick BBO crystal with phase-matching considerations oriented for type I degenerate PDC.

The PDC source produced pairs of horizontally polarized photons at 814 nm, which were coupled into a single-mode 3-dB fiber coupler (e.g., a 50:50 fiber beamsplitter) that formed the front half of a fiber-based PDC MZ interferometer. Each arm of the PDC MZ contained a fiber-coupled adjustable air gap optical delay line (OZ Optics, Model ODL 200). These delay lines had a travel range of 25 mm, and could be used to adjust the relative path lengths in the device.

The back half of the PDC MZ was formed by a second 3-dB fiber coupler. The outputs of the PDC MZ were coupled back into free space, and passed through interference filters with a

10-nm full width at half maximum centered at 814 nm. Two single-photon detectors and standard coincidence-counting electronics were then used to record the data. Paddle-wheel-style fiber polarization controllers (FPC's) were used in several locations to control the polarizations in the experiments. The entire fiber-based PDC MZ interferometer was built on a large 0.5-in.-thick aluminum plate contained within a heavily insulated box to provide passive thermal stability and minimize phase drift.

In order to match the 60-cm free-space path-length imbalance of the pump MZ, an extra ~ 40 cm of fiber was added to the long arm of the fiber-based PDC MZ interferometer. To ensure that τ exactly matched τ_p , we temporarily connected the pump MZ directly in series with the PDC MZ and used an auxiliary broadband “white-light” source as the input. Small adjustments to the air-gap delay lines were then made to find first-order interference and match the optical delays in the two interferometers.

IV. PUMP MZ STABILITY TESTS

As can be seen from Eq. (2), the coincidence counting rate depends on both ϕ and ϕ_p . Because we are interested in two-photon interference effects in the PDC MZ, it was necessary to ensure that ϕ_p was held stable while ϕ was scanned in a controlled way. We therefore conducted a number of auxiliary tests to verify the stability of the pump MZ and the ability to scan ϕ .

In practice, we passively scanned ϕ using a thermally induced phase drift. As shown in Fig. 2, a resistive heating element was used on a small segment (~ 5 cm) of fiber in the short arm of the PDC MZ. We developed a procedure in which the heating element's temperature was raised 4° and

then quickly turned off. After approximately 20 minutes into the subsequent cooling process, the PDC MZ interferometer drifted fairly linearly as a function of time, and went through roughly three 407-nm de Broglie periods in about 15 minutes. The entire free-space pump MZ interferometer was kept inside a simple noninsulated hardboard box to minimize air current and thermal disturbances. This kept the pump interferometer relatively stable, and there was negligible phase drift in ϕ_p over a time period much longer than the 15 minutes needed to scan ϕ through several fringes.

In order to verify the long-term stability of the pump MZ, we used the auxiliary narrow-band external-cavity diode laser setup shown in the top part of Fig. 2. The same laser setup could also be used to roughly calibrate the heating procedure used for scanning ϕ in the PDC MZ interferometer. The laser (New Focus Inc. Velocity Model 6312) had a linewidth <300 KHz and a coherence length that greatly exceeded the optical path-length imbalance of both the pump and PDC MZ interferometers. As shown in Fig. 2, a standard feedback loop based on an absorption measurement in a Rubidium vapor cell was used to stabilize the wavelength of the laser. We typically locked the laser's frequency to within 20 MHz of one of the ground-state hyperfine levels of the D_2 transition near 780 nm [26]. The locking was performed every 25 ms, which was frequent enough to prevent this particular laser from drifting more than $\sim 10^{-6}$ wavelengths from a fixed value. This locking procedure kept any phase noise due to wavelength drift to a negligible level during our tests.

Figure 3 shows results from a typical stability test based on first-order interference measurements in the pump MZ interferometer. A dichroic mirror was temporarily added to inject

both the 780-nm laser, as well as the 407-nm pump laser, into the pump MZ. The 780-nm light was monitored by a detector in the lower output port of the pump MZ, while the 407-nm light was simultaneously monitored by a detector placed in the output of the single-mode pump fiber. To demonstrate the stability, the data shown in Fig. 3 were recorded just after an intentional disturbance to the pump MZ with a heat gun. The 780-nm signal (black trace) shows nearly 100% first-order interference fringes that die out as the effects of the disturbance wear off. After ~ 1 hour, the phase drift is seen to be negligible. Multiple data runs under slightly different conditions showed the same type of behavior, with minimal phase drifts after the interferometer had stabilized. During our main experiments, we typically started collecting PDC data after the pump MZ box had been sealed for many hours, from which we expect a negligible ϕ_p phase drift over a 15-minute data collection period.

The second data set [red (grey) trace] shown in Fig. 3 corresponds to the 407-nm pump signal collected during the same time interval as the 780-nm auxiliary laser signal (black trace). The key point here was to demonstrate the minimal amount of first-order coherence displayed by the pump laser, as desired for our experiments. We ensured that the polarizations of the pump laser from both arms of the interferometer were the same, and measured the contribution of the total power coupled into the single-mode pump fiber to be roughly 60% from the short arm, and 40% from the long arm (this deviated from the ideal 50:50 split due to minor deviations in beamsplitter reflectivities and fiber-coupling efficiencies). These conditions predict a maximal visibility of 98% for a long-coherence-length source, whereas the visibility of the [red (grey) trace] in Fig. 3 is only roughly 8% for our short-coherence-length 407-nm diode pump laser.

Although the 60-cm path-length imbalance of the pump MZ greatly exceeds the expected coherence length of the pump, it is well known that the output of a CW multimode diode laser can exhibit multiple “peaks” separated by a distance $2L$, where L is the length of the laser cavity [27,28]. In fact, two-photon interference experiments have been performed where the interference originates from the coherence between these types of recurring peaks [8,9]. In contrast, the two-photon interference effects of interest in our setup should be due to second-order coherence induced by the pump MZ, rather than the laser itself [7]. Consequently, we needed to verify that the 407-nm pump laser exhibited the kind of minimal first-order interference seen in the [red (grey) trace] of Fig. 3.

We also performed an auxiliary Michelson interferometer test [28] on our 407-nm laser and found the spacing between the recurring diode laser peaks to be $(4705.5 \pm 0.9) \mu\text{m}$. The path-length imbalance of the pump MZ therefore corresponds to a separation on the order of 100 peaks. Coherence between these widely spaced peaks is possible, but unlikely to be large due to the finite linewidths of the individual modes in the diode laser [29]. At the same time, the ~ 60 -cm path-length imbalance was not intentionally set to exactly match a whole number of peaks. We believe that a combination of these two effects nearly eliminated the first-order pump interference in the [red (grey) trace] of Fig. 3, as desired.

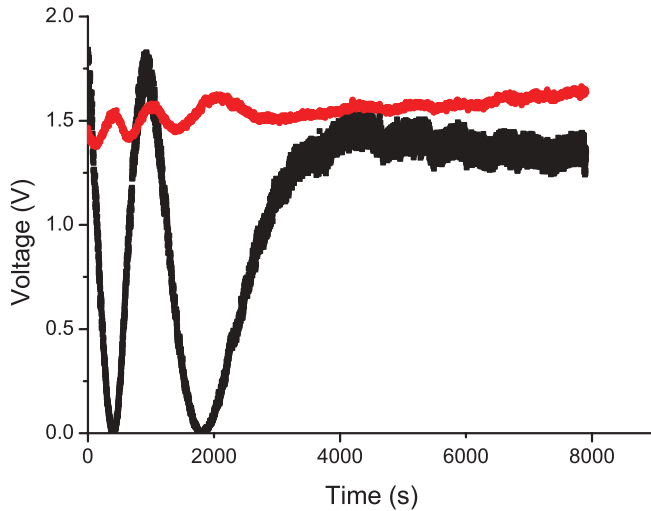


FIG. 3. (Color online) Typical results of a stability test of the pump Mach-Zehnder interferometer. The long-coherence-length auxiliary laser at 780 nm and the pump laser at 407 nm are simultaneously sent through the pump interferometer. Detectors monitor their outputs after an intentional large thermal disturbance to the interferometer. The auxiliary 780-nm signal (black trace) demonstrates the required stability of the pump interferometer phase during the experiments of interest, while the 407-nm signal [red (grey) trace] demonstrates a lack of significant first-order interference for the pump laser, as desired.

V. EXPERIMENTAL RESULTS

The results of our study can be best understood by considering four sequential experimental steps that were used to build up to the final conceptual diagram of Fig. 1. The results of these four steps are shown in Figs. 4–7.

In the first step, the HOM interference effects which generate the two-photon NOON state were optimized. To do this, the pump beam was sent directly into the pump fiber (and then the PDC crystal) without passing through a pump MZ interferometer. Additionally, the output ports of the first PDC 50:50 beamsplitter were connected directly to the detection channels, rather than serving as the inputs to the PDC MZ interferometer. In this way, a standard fiber-based HOM interferometer was temporarily formed [15]. In our setup, the relative delays between the two photons impinging on the HOM beamsplitter were controlled with translating glass wedges in the free-space paths after the PDC crystal, and FPC's on the input leads of the beamsplitter were used to ensure the polarization states of the PDC photons were the same.

Figure 4 shows the results of a typical HOM test in our setup. The data show a plot of the coincidence count rate as a function of the relative optical delay between the two incident photons, with the expected HOM “dip” at zero time delay. The data are best fit by a dip function with a visibility $(97.8 \pm 0.4)\%$ which signifies that both photons nearly always exit through the same output port of the beamsplitter. This ensures a high-fidelity two-photon NOON state, which is crucial for our subsequent experiments. Any contamination by terms corresponding to one photon in each output path of this first beamsplitter would lead to unwanted $|L_s S_i\rangle$ amplitudes, which are assumed to be nonexistent in our analysis of the full PDC MZ interferometer.

In the second step of the procedure, the outputs of the first 50:50 beamsplitter were reconnected as shown in Fig. 2

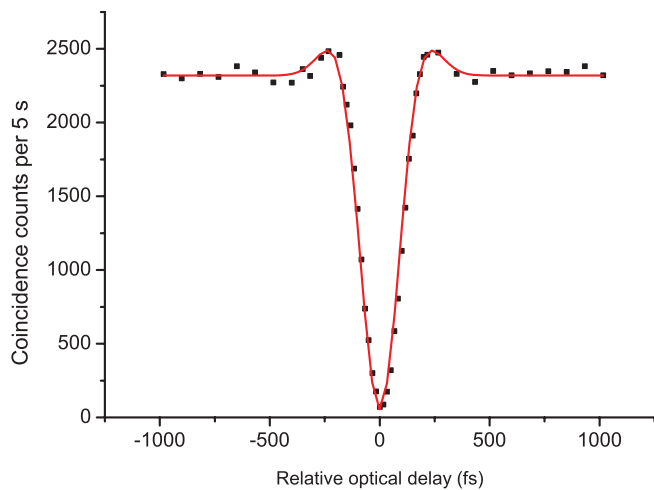


FIG. 4. (Color online) Results from the first step of the experimental procedure showing the expected Hong-Ou-Mandel dip [15,16] with a $(97.8 \pm 0.4)\%$ visibility. This indicates a high-fidelity NOON state in the output ports, as desired. The small shoulders in the data and fit are due to the fact that the 10-nm bandpass filters used in front of the detectors have a transmission profile that slightly deviates from a Gaussian shape.

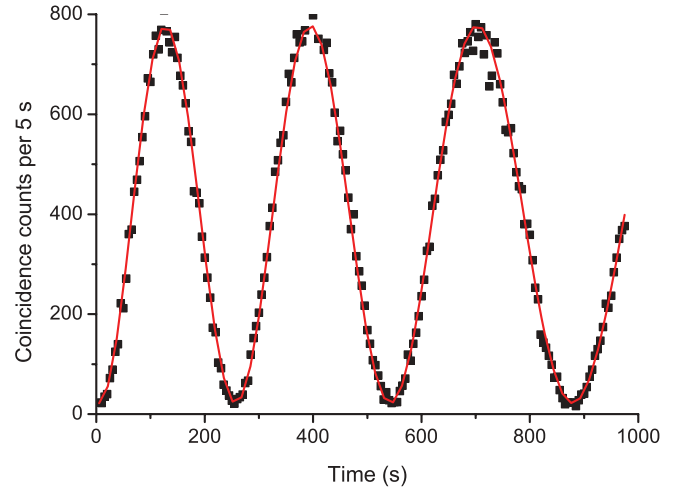


FIG. 5. (Color online) Results from the second step of the experimental procedure showing two-photon interference with a balanced PDC MZ interferometer and no pump MZ interferometer. In this step, the arrangement is functionally equivalent to the well-known Rarity interferometer [18]. The data shows a sinusoidal variation in the coincidence counting rate as a function of time during a thermally induced passive phase scan, with a best-fit visibility of $(93.0 \pm 0.7)\%$.

to form the full PDC MZ interferometer. However, the extra 40-cm-long fiber was not yet installed in the upper arm, so the two arms of the PDC MZ are exactly balanced. Again, the pump MZ interferometer was not used. In this configuration, our setup essentially reproduced the original two-photon MZ interference experiment of Rarity *et al.* [18]. Although we are using a short-coherence-length CW pump, the fact that the PDC MZ is balanced allows 100% visibility de Broglie wavelength fringes to be observed in the coincidence counting rate [18]. This test allowed us to verify our phase-scanning procedure and estimate the limitations on the visibility due to mode-matching and other technical issues in our apparatus.

Figure 5 shows the results of this test when the relative phase in the balanced PDC MZ interferometer was passively scanned using the fiber-heating procedure described in Sec. IV. The data show the expected sinusoidal variation in the coincidence counting rate as a function of time. The maximum value points correspond to relative phase differences that are even multiples of 2π , where constructive two-photon interference deterministically splits the two-photon NOON state into exactly one photon in each output port of the PDC MZ. This is simply the time reverse of the HOM effect [30,31]. The slight “stretching” of the sinusoidal data in Fig. 5 is due to the fact that the relative phase drift is not exactly linear with time, as would be expected from passive cooling of the heated-fiber segment during this time interval. The data are best fit by a sinusoidal function that takes this stretching into account, with a visibility of $(93.0 \pm 0.7)\%$. This high visibility indicates a good degree of indistinguishability between the interfering two-photon amplitudes, and that phase instabilities during each 5-second coincidence-collection point are not a significant source of error in our setup.

The third step of the procedure involved repeating the same type of scan shown in Fig. 5, but with the extra 40-cm segment of fiber installed in the upper arm of the PDC interferometer. In

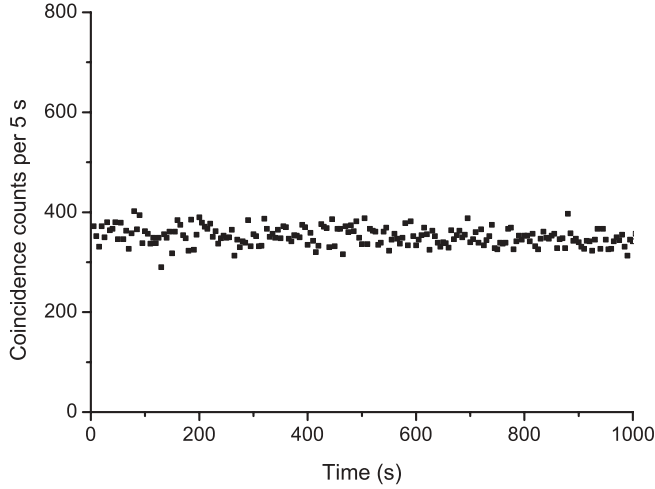


FIG. 6. Repeat of the data scan in Fig. 5, but with the PDC MZ interferometer path-length difference intentionally set to be much larger than the coherence length of the pump laser. Under these unbalanced conditions, the two-photon interference effects seen in Fig. 5 are completely washed out, as expected.

this case, the path-length imbalance of the PDC interferometer greatly exceeds the coherence length of the pump laser. Consequently, there is no coherence between the $|S_s S_i\rangle$ and $|L_s L_i\rangle$ amplitudes, and no two-photon interference is expected [6,18]. Figure 6 shows a result of the data accumulated in this configuration under the same scanning procedure used for Fig. 5. It can be easily seen that the high-visibility two-photon interference fringes of Fig. 5 have completely vanished due to the short coherence length of the pump laser.

The fourth and final step is to partially recover these lost two-photon interference effects by passing the pumping laser through the free-space pump MZ interferometer shown in Fig. 2, with its path-length imbalance set equal to the path-length imbalance of the PDC MZ (e.g., $\tau_p = \tau$). As described in Sec. II, the use of the pump MZ divides the two interfering two-photon amplitudes into the four indistinguishable amplitudes of Eq. (1). Two of these four amplitudes are coherent in analogy with pulsed time-bin experiments [7], while the two remaining incoherent amplitudes cannot be cut off due to the CW nature of the pump. This allows a partial recovery of two-photon interference, with a theoretical maximum visibility of 50% given by Eq. (2).

Figure 7 shows the results of this final step when the relative phase ϕ_p of the pump MZ was stabilized, and the relative phase ϕ of the PDC MZ was scanned by the same fiber-heating procedure used in Figs. 5 and 6. The data show the predicted sinusoidally varying coincidence counting rate, with a best-fit visibility of $(40.8 \pm 0.5)\%$. The recovered two-photon interference fringes seen in Fig. 7 represent the primary experimental result of this paper.

Note that due to the lack of significant first-order interference in the pump MZ interferometer, only half of the original pump laser power is delivered to pump fiber (and then the PDC crystal), while the other half is wasted through the lower output port of the second 50:50 beamsplitter in the pump MZ. Consequently, the average coincidence counting rate in Fig. 7

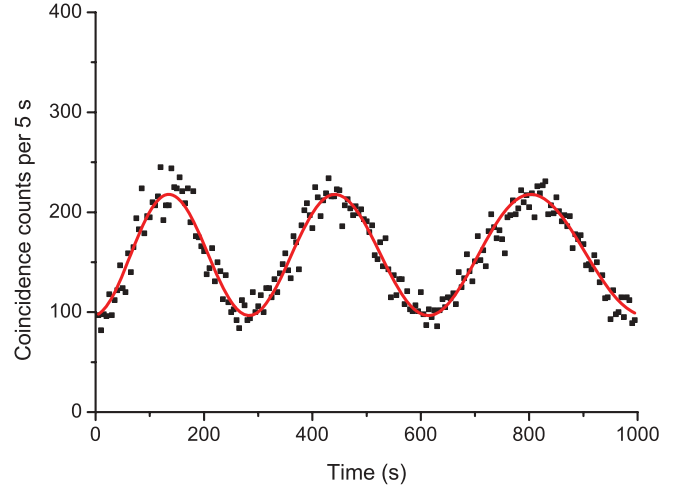


FIG. 7. (Color online) Primary experimental results obtained by using the pump MZ interferometer with its path-length imbalance set to exactly match that of the PDC MZ interferometer. This represents data taken with the complete setup shown in Fig. 2. As described in the discussion of Fig. 1, the inclusion of the pump MZ allows a recovery of two-photon interference with a theoretical maximum visibility of 50%. The experimental data are fit by a sinusoidal function with a $(40.8 \pm 0.5)\%$ visibility.

is roughly half of those seen in Figs. 5 and 6. Additionally, the apparent de Broglie wavelengths in Figs. 5 and 7 are slightly different because the heating procedure used to implement a phase scan is not actively controlled, and varies slightly from run to run.

Furthermore, the 93% visibility of Fig. 5 obtained with a balanced Rarity MZ setup [18] should ideally translate to a 46.5% visibility in the data of Fig. 7. We believe the reduction to 40.8% in the actual experiment is primarily due to alignment sensitivity in the HOM effect and PDC MZ interferometer, rather than any phase instability in the pump MZ interferometer. Additionally, the nonideal 60:40 splitting of the pump MZ interferometer led to a visibility loss of only 1% due to a slightly unequal weighting of the interfering $|S_p; L_s L_i\rangle$ and $|L_p; S_s S_i\rangle$ amplitudes in Eq. (1), and was not a major factor. Despite these issues, the primary results shown in Fig. 7 clearly demonstrate the expected interference fringes that can be obtained in this intermediate regime of two-photon interferometry with a short-coherence-length CW pump laser.

The maximum expected two-photon interference fringe visibility of only 50%, and the use of only a single common PDC MZ interferometer (as opposed to two spatially separated PDC MZ interferometers [6,7]), raises the valid question of classical analogs that could simulate the results of Fig. 7 [32–34]. Indeed a single balanced “PDC MZ” interferometer fed by a variety of simple classical light sources can produce 100% visibility fringes in the product of photodiode signals from its output ports. The fact that we are essentially using two unbalanced (but matched) MZ interferometers in series does not fundamentally change the situation, and opens the possibility of classical white-light-type interference effects that can produce results related to Fig. 7.

VI. SUMMARY AND DISCUSSION

In some sense, the interference effects observed in PDC-based two-photon interferometry originate from the uncertainty in the emission time of the detected photon pair. In the original Franson-type experiments [6], the use of a narrow-band CW pump laser renders the photon pair emission time completely uncertain, while in the Gisin-type pulsed time-bin experiments the emission time is confined to two possible well-defined values [7]. In both cases, however, the fact that the two-photon state is a coherent superposition of the possible emission times allows high-visibility nonclassical interference effects to be observed. In this paper, we have described an experimental demonstration of an intermediate situation that shares features of both of these extreme cases.

By passing a short-coherence-length CW pump laser through an unbalanced time-bin-like pump MZ interferometer, coherence is created between two possible pair emission times with a well-defined separation, but an unknown overall starting time. As in the pulsed time-bin case, this coherence allows two-photon interference effects to be seen in a subsequent

unbalanced PDC MZ interferometer, regardless of the coherence properties of the pump laser itself [7]. However, the CW nature of the pumping beam here precludes the use of the convenient “starting clock” available in the pulsed-pump case. This prevents the ability to cut off incoherent two-photon amplitudes which limits the visibility to 50% here, as opposed to the 100% visibility that is possible in the pulsed case [7].

The observation of these effects was facilitated by using a two-photon NOON state in a single fiber-based unbalanced PDC MZ interferometer [18]. In comparison to more general experiments using two spatially separated PDC MZ interferometers [6,7], this provided a relatively robust and stable experimental platform for an explicit demonstration the role of pump coherence in an intermediate regime of two-photon interferometry.

ACKNOWLEDGMENTS

We acknowledge useful discussions with our colleague J. D. Franson. This work was supported in part by the National Science Foundation under Grant No. 0652560.

-
- [1] M. D’Angelo, M. V. Chekhova, and Y. H. Shih, *Phys. Rev. Lett.* **87**, 013602 (2001).
 - [2] V. Giovannetti, S. Lloyd, and L. Maccone, *Science* **306**, 1330 (2004).
 - [3] A. K. Ekert, J. G. Rarity, P. R. Tapster, and G. Massimo Palma, *Phys. Rev. Lett.* **69**, 1293 (1992).
 - [4] D. M. Greenberger, M. A. Horne, and A. Zeilinger, *Physics Today* **46**, 22 (1993).
 - [5] D. N. Klyshko, *Photons and Nonlinear Optics* (Gordon and Breach, Amsterdam, 1988).
 - [6] J. D. Franson, *Phys. Rev. Lett.* **62**, 2205 (1989).
 - [7] J. Brendel, N. Gisin, W. Tittel, and H. Zbinden, *Phys. Rev. Lett.* **82**, 2594 (1999).
 - [8] A. V. Burlakov, M. V. Chekhova, O. A. Karabutova, and S. P. Kulik, *Phys. Rev. A* **63**, 053801 (2001).
 - [9] O. Kwon, Y.-S. Ra, and Y.-H. Kim, *Opt. Express* **17**, 13059 (2009).
 - [10] T. E. Keller and M. H. Rubin, *Phys. Rev. A* **56**, 1534 (1997).
 - [11] Y.-H. Kim, M. V. Chekhova, S. P. Kulik, and Y. H. Shih, *Phys. Rev. A* **60**, R37 (1999).
 - [12] Y.-H. Kim, V. Berardi, M. V. Chekhova, A. Garuccio, and Y. H. Shih, *Phys. Rev. A* **62**, 043820 (2000).
 - [13] H. de Riedmatten, I. Marcikic, V. Scarani, W. Tittel, H. Zbinden, and N. Gisin, *Phys. Rev. A* **69**, 050304 (2004).
 - [14] D. Stucki, H. Zbinden, and N. Gisin, *J. Mod. Opt.* **52**, 2637 (2005).
 - [15] C. K. Hong, Z. Y. Ou, and L. Mandel, *Phys. Rev. Lett.* **59**, 2044 (1987).
 - [16] Y. H. Shih and C. O. Alley, *Phys. Rev. Lett.* **61**, 2921 (1988).
 - [17] A. N. Boto, P. Kok, D. S. Abrams, S. L. Braunstein, C. P. Williams, and J. P. Dowling, *Phys. Rev. Lett.* **85**, 2733 (2000).
 - [18] J. G. Rarity, P. R. Tapster, E. Jakeman, T. Larchuk, R. A. Campos, M. C. Teich, and B. E. A. Saleh, *Phys. Rev. Lett.* **65**, 1348 (1990).
 - [19] J. D. Franson, *Phys. Rev. A* **44**, 4552 (1991).
 - [20] I. Marcikic, H. de Riedmatten, W. Tittel, H. Zbinden, M. Legre, and N. Gisin, *Phys. Rev. Lett.* **93**, 180502 (2004).
 - [21] P. G. Kwiat, W. A. Vareka, C. K. Hong, H. Nathel, and R. Y. Chiao, *Phys. Rev. A* **41**, 2910 (1990).
 - [22] J. Brendel, E. Mohler, and W. Martienssen, *Phys. Rev. Lett.* **66**, 1142 (1991).
 - [23] J. Jacobson, G. Bjork, I. Chuang, and Y. Yamamoto, *Phys. Rev. Lett.* **74**, 4835 (1995).
 - [24] E. J. S. Fonseca, C. H. Monken, and S. Padua, *Phys. Rev. Lett.* **82**, 2868 (1999).
 - [25] K. Edamatsu and R. Shimizu, *Phys. Rev. Lett.* **89**, 213601 (2002).
 - [26] [<http://steck.us/alkalidata/>], website maintained by D. A. Steck, University of Oregon.
 - [27] J. W. Goodman, *Statistical Optics* (Wiley, New York, 1985), p. 230.
 - [28] S.-Y. Baek, O. Kwon, and Y. H. Kim, *Jpn. J. Appl. Phys.* **46**, 7720 (2007).
 - [29] J. Rodriguez, A. Siahmakoun, G. Salamo, M. J. Miller, W. W. Clark III, G. L. Wood, E. J. Sharp, and R. R. Neurgaonkar, *Appl. Opt.* **26**, 1732 (1987).
 - [30] T. B. Pittman, B. C. Jacobs, and J. D. Franson, *New J. Phys.* **9**, 195 (2007).
 - [31] J. Chen, J. B. Altepeter, and P. Kumar, *New J. Phys.* **10**, 123019 (2008).
 - [32] Z. Y. Ou and L. Mandel, *J. Opt. Soc. Am. B* **7**, 2127 (1990).
 - [33] R. Kaltenbaek, J. Lavoie, and K. J. Resch, *Phys. Rev. Lett.* **102**, 243601 (2009).
 - [34] J. D. Franson, *Phys. Rev. A* **80**, 032119 (2009).